nature physics

ARTICLES

PUBLISHED ONLINE: 26 JULY 2009 | DOI: 10.1038/NPHYS1344

The nature of localization in graphene under quantum Hall conditions

J. Martin[1,2], N. Akerman[2], G. Ulbricht[3], T. Lohmann[3], K. von Klitzing[3], J. H. Smet[3] and A. Yacoby[1,2]*

Particle localization is an essential ingredient in quantum Hall physics. In conventional high-mobility two-dimensional electron systems such as in GaAs/AlGaAs semiconductor heterostructures, Coulomb interactions were shown to compete with disorder and to have a central role in particle localization. Here, we address the nature of localization in graphene where the carrier mobility, quantifying the disorder, is two to four orders of magnitude smaller than in GaAs two-dimensional electron systems. We image the electronic density of states and the localized state spectrum of a graphene flake in the quantum Hall regime with a scanning single-electron transistor. Our microscopic approach provides direct insight into the nature of localization. Surprisingly, despite strong disorder, our findings indicate that localization in graphene is not dominated by single-particle physics, but rather by a competition between the underlying disorder potential and the repulsive Coulomb interaction responsible for screening.

The quantum Hall effect is manifested in transport through vanishing longitudinal resistance and a quantized transverse resistance[1]. In graphene, the relativistic nature of the underlying particles and the absence of valley mixing give rise to quantum Hall phases at filling factors $\nu = 4i-2$, where the four-fold degeneracy is a result of both spin and valley degeneracies[2–4]. It is well established that disorder has a crucial role in the formation and robustness of quantum Hall phenomena[1,5]. Whereas at low magnetic fields the relativistic nature of the electronic spectrum of graphene prevents particle localization, the application of a strong magnetic field perpendicular to the layer opens up Landau gaps in the spectrum that lead to strong localization[6]. Clearly the universal nature of the quantum Hall effect in macroscopic specimens relies on its insensitivity to the details of the underlying disorder mechanism. Already single-particle physics of two-dimensional (2D) electrons in a disordered potential landscape leads to localization of charge and scaling behaviour[1,5]. However, in high-mobility GaAs specimens, localization is no longer solely driven by disorder and a fundamentally different picture of localization emerges that is strongly influenced by the presence of Coulomb interactions, leading to Coulomb blockade and nonlinear screening of the disorder potential[7–11].

Thus far, Coulomb interactions in clean 2D electron systems are known to have a profound effect and may bring about for example the fractional quantum Hall effect[12] and quantum Hall ferromagnetism. The latter was recently observed in graphene[13–17]. However, the carrier mobility in non-suspended graphene, a common measure of the disorder strength, is typically 10^3–10^4 times smaller than the mobility characterizing GaAs-based 2D systems[2,3,18–20]. Even in suspended layers, peak mobilities are up to a hundred times smaller than those measured in high-mobility GaAs layers[21,22]. It raises the question of whether Coulomb interactions have a significant role in particle localization in graphene or perhaps single-particle physics suffices. To address this issue, we explore the electronic density of states in graphene at high magnetic fields using a scanning single-electron transistor (SET). We focus our work on the quantum Hall regime, where we image the bands of localized states both in position and energy. Our findings clearly indicate that at large magnetic fields, charge localization is governed by the presence of strong Coulomb repulsion between electrons despite the high level of disorder and the behaviour is similar to the one observed in GaAs 2D electron systems with their much larger carrier mobilities.

The preparation of graphene monolayers was carried out in a similar manner to that reported in refs 23, 24. A detailed description is given in the Methods section. The sample was mounted in the preparation chamber of an ultrahigh vacuum scanning system and subsequently annealed by heating it above 100 °C at a background pressure of 5×10^{-7} mbar. The entire annealing procedure removed most of the doping adsorbates introduced during fabrication and exposure to humidity and the neutrality point shifted close to zero backgate voltage[25]. A backgate voltage difference of 1 V corresponds to a density change of 7×10^{10} cm^{-2}. This conversion factor was extracted from two-terminal magneto-transport data.

We begin our investigations by measuring the energy level diagram as a function of the applied external magnetic field and density. Using a scanning probe microscope equipped with a SET on a glass fibre tip, the local chemical potential μ and the inverse compressibility $\partial\mu/\partial n$ are recorded. The SET measures the local electrostatic potential. However, under equilibrium conditions, any changes in the local chemical potential are exactly compensated for by changes in the local electrostatic potential. Hence, the SET enables detection of the local chemical potential as well as its local derivative $\partial\mu/\partial n$ when weakly modulating the carrier density through the doped Si backgate. The latter quantity is inversely proportional to the local compressibility and directly related to the local density of states. The details of this technique have been described previously in refs 26, 27. Figure 1a shows a schematic diagram of the experimental arrangement with the SET hovering above the monolayer.

The energy spectrum of graphene can be determined by measuring the chemical potential as a function of the carrier density. In a fixed magnetic field and in the absence of disorder, the chemical potential undergoes sudden jumps equal to the energy between

[1]Department of Physics, Harvard University, Cambridge, Massachusetts 02138, USA, [2]Department of Condensed Matter Physics, Weizmann Institute of Science, Rehovot 76100, Israel, [3]Max-Planck-Institut für Festkörperforschung, Heisenbergstrasse 1, D-70569 Stuttgart, Germany.
*e-mail: yacoby@physics.harvard.edu.

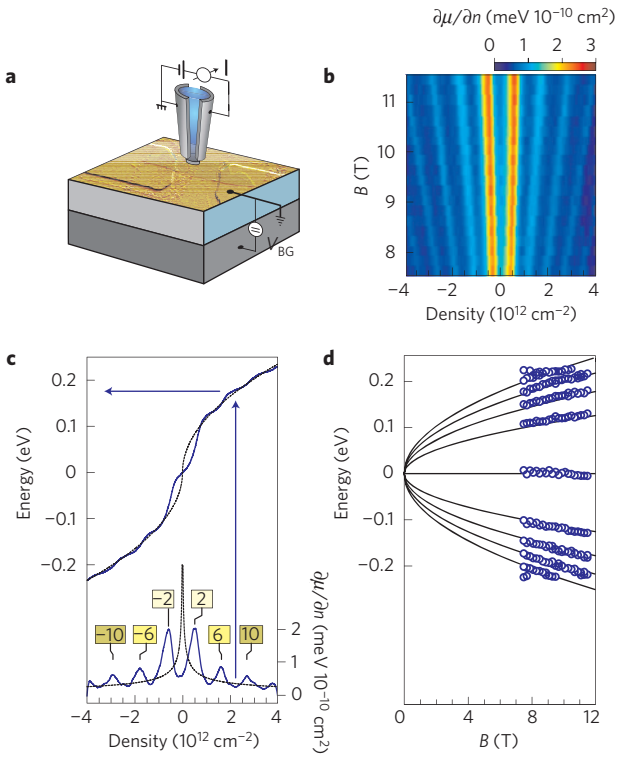

Figure 1 | The Landau-level spectrum in monolayer graphene extracted from compressibility measurements. a, Schematic diagram of the device geometry consisting of a graphene monolayer and a source and drain contact on top of a doped Si substrate covered by a 300-nm-thick thermal oxide. A scanning SET is hovering above the graphene sample at a distance of a few tens of nanometres. **b**, Colour rendition of the inverse compressibility $\partial\mu/\partial n$ in units of 10^{-10} meV cm^2 as a function of the applied magnetic field B and the carrier density n. **c**, Measured chemical potential μ (top curves) and inverse compressibility $\partial\mu/\partial n$ at a fixed field $B = 11.7$ T (solid lines) in comparison with the calculated behaviour of μ and $\partial\mu/\partial n$ at zero field (dotted lines). **d**, Landau-level energies as a function of the magnetic field extracted from the μ and $\partial\mu/\partial n$ measurements. The solid lines plot the Landau-level energies assuming a Fermi velocity $v_F = 1.1 \times 10^6$ m s^{-1}.

adjacent Landau levels. They arise when gradually increasing the density whenever the degeneracy of the highest filled Landau level is exhausted and the next Landau level starts to be filled. The chemical potential can either be measured directly with the SET or is obtained by integrating compressibility data. A colour rendition of the inverse compressibility as a function of magnetic field B and carrier density n for a fixed position on the graphene flake is shown in Fig. 1b. The gaps in the energy spectrum give rise to regions where the inverse compressibility is large. These regions appear as lines at filling factors $\nu = 4i - 2$ with $i = -1, 0, 1, 2\ldots$. Figure 1c shows a measurement of the chemical potential (top curve) together with a cross-section through the inverse compressibility data of Fig. 1b at a fixed magnetic field of 11.7 T. Prominent integer fillings have been marked. For the sake of comparison, the theoretical behaviour of the chemical potential and the inverse compressibility at zero magnetic field have been included as well (dotted lines). Substantial disorder broadening[28] in graphene is responsible for the absence of abrupt jumps in the chemical potential. Only a smooth undulation is observed when an extra Landau level gets filled. From these data, the Landau-level energy spectrum can be reconstructed. A maximum in the compressibility (or a minimum in the depicted inverse compressibility) heralds the centre of the individual Landau levels. The chemical potential values at the densities where such compressibility maxima appear yield the Landau-level positions on the energy axis. A slight refinement of this simple procedure to extract the energy spectrum is required owing to stray electric fields and is discussed in the Methods section. The resulting Landau-level spectrum after the stray field correction is plotted in Fig. 1d. A similar spectrum has recently been obtained from scanning tunnelling spectroscopy[29]. The energy of the centre of each Landau level agrees well with the expected theoretical value as given by $E_i = \mathrm{sgn}(i) \cdot \sqrt{2e\hbar v_F^2 |i| B}$. Here, i is the Landau level index ($i > 0$ for electron-like and $i < 0$ for hole-like Landau levels) and v_F is the Fermi velocity. A best fit to the data yields a Fermi velocity equal to $1.1 \pm 0.1 \times 10^6$ m s^{-1}, which differs only by 10% from the value expected from band-structure calculations[30]. This value is also consistent with our previous compressibility studies in the absence of a magnetic field from which a nearly identical value of the Fermi velocity was obtained[31]. Theoretical studies addressing disorder and interactions confirm such weak renormalization of the Fermi velocity[6,32,33].

The colour rendition in Fig. 1b provides an overall view of the behaviour of the local compressibility but does not provide enough resolution to observe the microscopic localized states. To observe localized states, we zoom into the individual incompressible regions by recording data on a much finer grid of the density versus magnetic field plane. The outcome is shown in Fig. 2a. Previous works on massive 2D electron systems made out of GaAs have shown that such local compressibility maps are dominated by sharp peaks that run parallel to the lines of constant integer filling when the system can still reach equilibrium on the timescale of the measurement[7]. Similar behaviour is seen here in graphene at large magnetic fields. Many dark lines or spikes that run parallel to the line of constant filling factor 2 and −2 are visible. Dark lines or spikes in the local compressibility reflect the charging with a single electron of a discrete localized state in close proximity to the SET. We will argue that these lines represent the charging spectra of the localized states induced by the ionized impurity potential. Below we show that the number of charging lines and their parallel character constitutes a direct proof that despite the strong disorder, localization in graphene is not a single-particle effect but rather involves an elaborate interplay between the disorder potential and local charge reorganization driven by the repulsive Coulomb interaction.

It is instructive to consider the expected behaviour of the localized state spectrum for strong disorder where one can neglect the effects of the Coulomb repulsion and screening first. Under these conditions, each localized state consists of a constant-energy contour of the disorder landscape. Each of these contours encloses an integer number of flux quanta. When the magnetic field increases, these constant-energy orbits must shrink in size to maintain a constant flux through their area and their energy changes accordingly within the Landau-level. For the sake of simplicity, we will restrict our discussion to the case where one Landau level is occupied. We will also assume that the characteristic length scale of the disorder is larger than the magnetic length. The Landau level will then develop spatial variations that are identical to the disorder potential. This assumption will be justified a posteriori. We note however that even if this assumption is not satisfied in experiment, it would not alter our conclusions. Figure 3a shows a random disorder potential and two sets of localized states at different locations. The larger of each pair of contours corresponds to the localized state at field B_1. The smaller contours illustrate how these localized states shrink as the field is raised from B_1 to B_2. Figure 3b plots a vertical cross-section through the disorder potential. It highlights how the energy of these localized states moves within the Landau level on increasing the field. For a particular localized state, the filling factor or average sample density at which it becomes populated depends on the specific details of the disorder landscape. In the density versus magnetic-field plane, this density does not

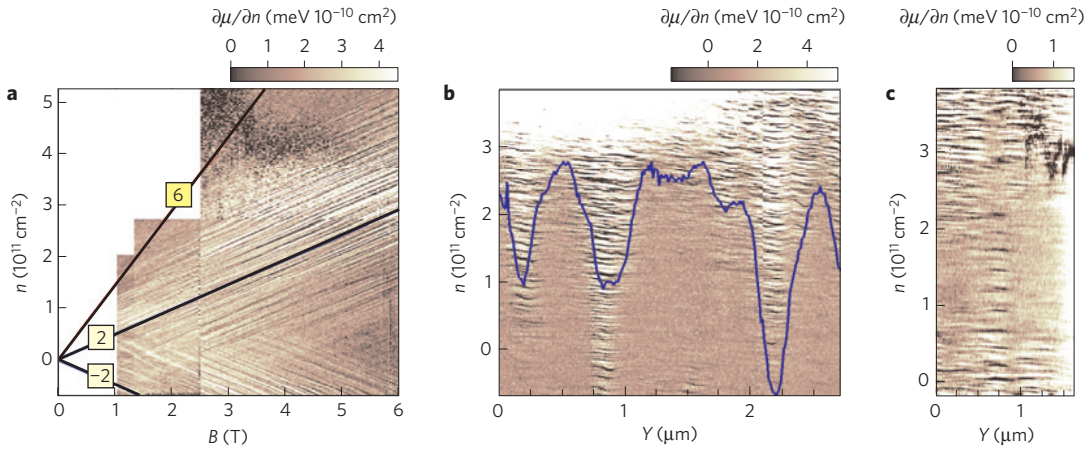

Figure 2 | Measured spectrum of localized states in graphene. a, Colour rendition of the inverse compressibility measured as a function of average carrier density (controlled using the backgate) and external magnetic field. The measurement is taken at a single location above the flake. Localized states in this measurement appear as dark lines that run parallel to the filling factor. **b**, Colour rendition of the inverse compressibility measured along a line across the graphene flake and as a function of average carrier density. Localized states in this measurement appear as dark horizontal lines spanning a small spatial extent determined by the localization length or by the resolution limit of the tip. The solid line indicates the carrier density profile along the same line extracted from the surface potential measurements. The data were taken at $B = 10$ T. **c**, Localized state spectrum of a single dot. The level spacing is inversely proportional to the size of the dot and yields a measured dot size of 60 nm. The data were taken at $B = 11$ T.

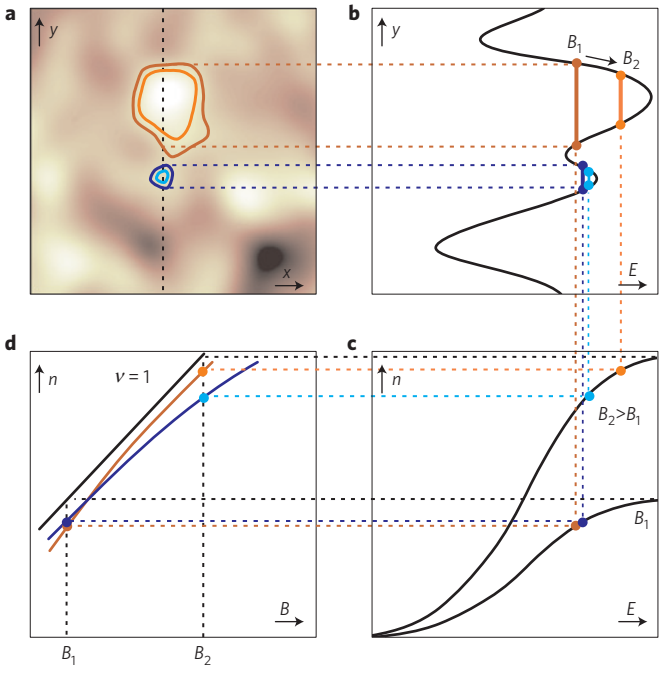

Figure 3 | Single-particle picture of localization in a perpendicular magnetic field. For the sake of simplicity, only one non-degenerate Landau level is considered. **a**, Example of a bare disorder potential with hills and valleys. Localized states correspond to orbits of constant energy that enclose an integer number of flux quanta. When increasing the field ($B_2 > B_1$), these constant-energy orbits shrink in size to maintain constant flux. Their energy may drop or increase depending on the details of the disorder potential. Their number increases in proportion to the increase in the level degeneracy per unit area $n_{max} = eB/h$. **b**, Cross-section through the disorder potential. The localized states shown in **a** are also highlighted here. **c**, Plot of the position of the chemical potential as a function of the average carrier density n in the Landau level for two values of the field B_1 and B_2. At large values of the chemical potential, the density approaches the level degeneracy n_{max}. **d**, Diagram plotting when each localized state becomes populated in the (n, B) plane. Population of a state causes a spike in the local compressibility.

necessarily evolve monotonically in magnetic field. In addition, as the magnetic field increases, the number of localized states should increase at any given location across the sample in proportion to the Landau-level degeneracy per unit area. The Landau-level degeneracy has increased in view of the larger number of flux quanta that now thread the sample. These key features of the single-particle picture of localization in the strong-disorder regime are illustrated schematically in Fig. 3c,d. For simplicity, the Landau-level spin and valley degeneracies are ignored and the filling of only one Landau level is shown. Figure 3c plots at a given field the average number of occupied states per unit area n in the Landau level as function of E. Furthermore, the density at which the localized states shown in Fig. 3a,b get filled are marked. Finally, Fig. 3d highlights the evolution of the two selected localized states in the (n, B) plane. The traces of adjacent localized states may 'cross' and they do not run parallel to the line corresponding to complete filling of the Landau level. We note that although the SET is a local probe it will nonetheless pick up the signature of all localized states within a spatial extent given by its size (of order 100 nm). We can therefore test exactly the above scenario, that is, whether localized states cross or not. We conclude that the generic features of single-particle localization such as the increase in the number of localized states with increasing field and their erratic, non-monotonic behaviour in the (n, B) plane are entirely absent in the data of Fig. 2a. Clearly, this picture does not hold for localization in graphene.

The behaviour of the localized state spectrum described above should be contrasted with the expected behaviour if Coulomb repulsion is strong enough to compete with disorder and to enforce local charge rearrangements to screen the bare disorder potential. We constrain our discussion to the framework of Thomas–Fermi screening and Coulomb blockade physics. Further effects of electron–electron interactions are beyond the scope of this article. A major contribution to the disorder potential arises from random charge impurities in the vicinity of the graphene sheet[34]. In agreement with scanning SET experiments[31], recent scanning tunnelling microscopy studies have confirmed the importance of random charge impurities producing a disorder length scale in the range of several to tens of nanometres[35,36]. Despite this relatively short length scale, theoretical estimates of the screening length are in the range of only a few nanometres[33], comparable to or smaller than the disorder length. In addition, even at magnetic

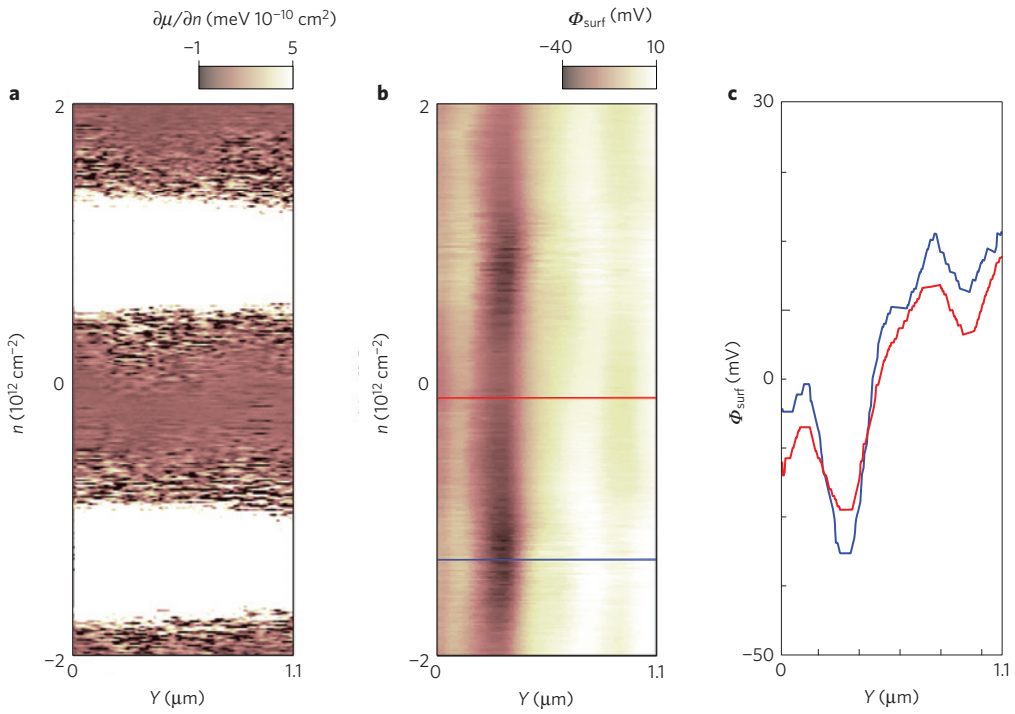

Figure 4 | The dependence of the measured electrostatic potential on the compressibility of graphene. a, Position–density scan of the inverse compressibility. Incompressible regions (white stripes) correspond to filling factor ± 2. $B = 11$ T. **b**, Simultaneously recorded electrostatic surface potential. Spatial potential fluctuations are enhanced in incompressible regions. **c**, Line scans taken from Fig. 5b in a compressible regime near zero density (red) and in the centre of an incompressible strip (blue). The remaining disorder potential in the compressible regime is mostly due to charge impurities on the top surface of the graphene sheet. The charges on the top surface cause a direct gating effect on the SET and are only marginally screened by the underlying graphene (for a detailed discussion, see Supplementary Information of ref. 31).

fields of only a few teslas, the magnetic length is comparable to the disorder length (that is, at $B = 4$ T, $l_B = 12.5$ nm). It is therefore expected that far away from complete filling of the Landau level, the electrons manage to flatten the potential by setting up a spatially varying density profile. The electrons succeed in screening the bare disorder potential because many states are available to rearrange electrons in the partially filled Landau level[33]. However, as one approaches a complete integer filling, the degeneracy n_{max} of the partially filled Landau level may get exhausted locally and electrons there can no longer rearrange to flatten the disorder potential. A direct measurement of the effective disorder potential as the density is changed is shown in Fig. 4. In incompressible regions, screening is poor and the remaining disorder potential is significantly larger than in a compressible region. Figure 5 illustrates this scenario in more detail. Regions where the electron density is still smaller than n_{max} remain compressible. Regions where the electron density equals the Landau-level degeneracy n_{max} are incompressible and the disorder potential is not screened. Close to complete filling of a Landau level, antidots or dots, surrounded by these incompressible regions, form as illustrated in Fig. 5a and Coulomb blockade physics becomes relevant. As the bare disorder remains fixed and independent of field, the same landscape of dots and antidots recurs at any field. In Fig. 5b, for instance, the magnetic field was increased. The Landau-level degeneracy n_{max} has gone up accordingly. The same antidots and localized states appear at higher density. Hence, the localized state spectra of the dots/antidots produce parallel lines in the (n, B) plane (Fig. 5c), rather than erratic, non-monotonic lines as in the single-particle model. This behaviour of the localized states can serve as a fingerprint of the interacting model for particle localization. It is well pronounced in the data recorded on graphene in Fig. 2a. Moreover, the same set of localized states would also reappear at different filling factors as well. Therefore, the number of

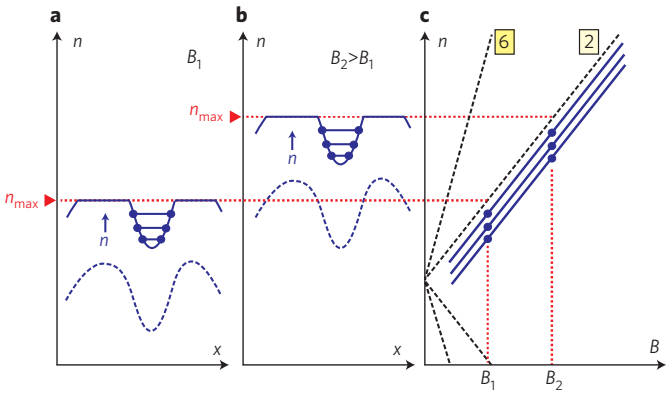

Figure 5 | The behaviour of localized states in the presence of nonlinear screening due to Coulomb repulsion. a, Electrons rearrange and set-up a spatially varying density distribution (dotted line) to flatten the bare disorder potential. This is possible as long as the required local charge density is smaller than the level degeneracy: n_{max}. Close to complete filling of the level, the level degeneracy may get locally exhausted. The density profile will exhibit isolated pockets of unfilled states or so-called antidots as shown here (solid blue line). Their charging involves Coulomb blockade physics and gives rise to compressibility spikes. **b**, At different magnetic fields, the same pockets of unfilled states will recur for the same distance in density from the n_{max} line. **c**. Owing to this recurrence, each localized state in the (B, n) plane gives rise to a line that runs parallel to the line of complete filling $n = n_{max}$ (or $\nu = 1$).

localized states and the width measured along the density ordinate of the incompressible band is expected to remain fixed independent of field and filling factor, provided that Landau levels are well separated. In Fig. 6, we plot the width in density of the band of

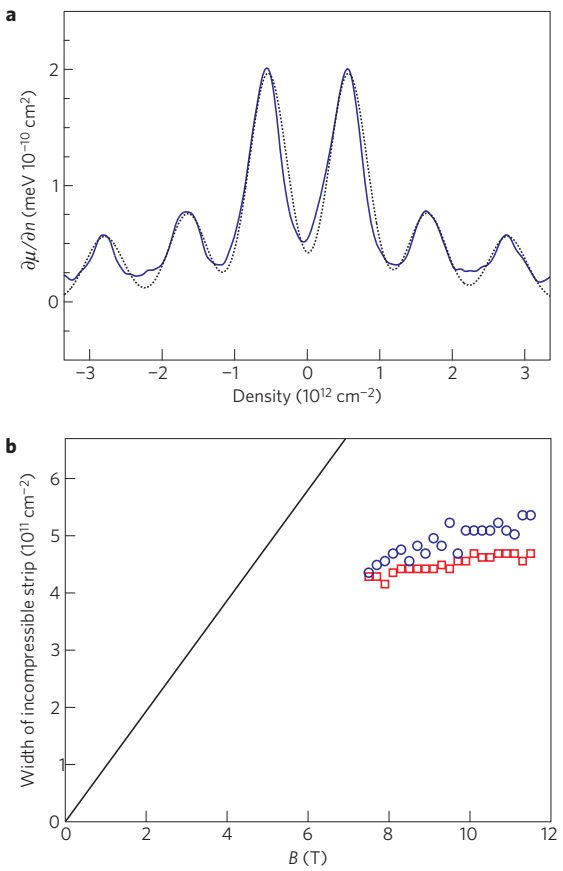

Figure 6 | The magnetic-field dependence of the width in density of the incompressible region. a, The width of the incompressible region is determined from a best fit to the data. The fit function is composed of Lorentzians centred at the maxima of the inverse compressibility. The variance of the Lorentzian serves as the fit parameter and is taken identical for all Lorentzians. A fit example is shown for the compressibility data recorded at 11.3 T. **b**, The dependence of the density width of the incompressible region on the applied magnetic field. These widths are extracted as described under **a**. A sum of Lorentzians (blue circles) as well as Gaussians (red squares) have been used. The solid line corresponds to $4eB/h$ and demarcates the transition from the regime of separated to overlapping levels.

localized states centred around integer filling as a function of magnetic field. For a given magnetic field, empirically we find that this width can be extracted well by fitting either a sum of Lorentzian or Gaussian functions to the inverse compressibility trace as illustrated in Fig. 6a. A Lorentzian (Gaussian) is centred at each integer filling where a maximum appears. The width or variance is assumed identical for all Lorentzians (Gaussians). This fitting procedure works well as long as Landau levels are well separated. Figure 6b clearly demonstrates that as the field increases and the separation between the Landau levels starts to exceed the broadening, the width of the incompressible band is saturating to a constant, magnetic-field-independent value. It corroborates further that Coulomb interactions and nonlinear screening are crucial ingredients for localization in graphene under quantum Hall conditions.

Up to this point, measurements were restricted to a single location. Figure 2b shows a colour rendition of the inverse compressibility recorded along a line across the graphene flake as a function of the average sample density (or equivalently filling factor) at $B = 10$ T. It reveals the spatial dependence of the charging spectrum and the bottom border of the incompressible band centred around filling factor 2. The charging of each localized state is now seen to persist over a finite spatial extent, which is set either by the localization length or by the resolution limit given by the size of the tip (∼100 nm). One can clearly see that electrons tend to localize at particular locations in space. We anticipate a strong correlation between these local density variations and the border of the incompressible band. It was shown previously that with a scanning SET it is also possible to extract the local density from a differential measurement of the surface potential in the compressible and incompressible regime[31]. The outcome of such a measurement has been included in Fig. 2b as the blue trace. For the incompressible behaviour, we used a Landau filling factor of 2 at an average density of about 3.5×10^{11} cm^{-2}. The surface potential measurement in the compressible regime was carried out at the centre of the Landau level at the charge neutrality point for a field of 10 T. The correspondence between the density fluctuations and the border of the incompressible band, that is, the appearance of localized states, is striking.

The typical length scale of the density fluctuations in the line scan of Fig. 2b is around 150 nm. It is resolution limited by the size of the SET sensor. The intrinsic disorder length scale of graphene was reported previously from the density interval spanned by the incompressible band around any of the well-resolved integer filling factors[31]. It was estimated to be approximately equal to 30 nm. A detailed study of spatial maps of the localized states spectra as in Fig. 2b offers however an alternative approach to estimate the characteristic length scale of the disorder. The level spacing between the localized states from a single dot or antidot is intimately connected to its size. Figure 2c shows one example of a spectrum of equidistant compressibility spikes that apparently stems from a single dot. It exhibits large level spacing. To add one extra electron to this dot, the average density in the sample needs to be changed by approximately 3×10^{10} cm^{-2}. Hence, the electron is localized within an area with a diameter of approximately 60 nm. This size fits reasonably well with the previously reported estimated length scale from the width of the incompressible band.

Methods

Sample preparation. An adhesive tape was used to peel a large graphite flake from a highly ordered pyrolytic graphite crystal. It was pressed onto a Si/SiO_2 wafer. The conducting Si substrate served as a backgate to vary the carrier density in the graphene sheet. Once a suitable monolayer was identified in an optical microscope, two electrical contacts were patterned with optical lithography. Typical dimensions of the monolayers were $10 \times 4\,\mu m^2$. After lift-off of the ohmic contact metal (3 nm Cr, 30 nm Au), the graphene flakes exhibited their neutrality point at backgate voltages larger than 100 V. Therefore, the sample surface was cleaned during an ozone treatment and with an ammonia dip. As-prepared flakes had their neutrality point at backgate voltages near 30 V. The sample was annealed by heating it above 100 °C at a background pressure of 5×10^{-7} mbar in the ultrahigh-vacuum scanning system. This procedure apparently removed the doping adsorbents introduced during fabrication and exposure to humidity and the charge neutrality point shifted close to zero backgate voltage.

Extraction of the Landau-level spectrum. The procedure to extract the Landau-level spectrum requires some refinement as some electrical field lines originating from the backgate reach the SET. The parasitic charge associated with these fringing fields is also detected by the SET. The detected amount of charge depends both on the distance of the SET to the graphene edge as well as on the vertical distance between the tip and the flake. For the heights and distances to the sample edge used in these experiments, we derive a contribution to the compressibility from the fringing fields of approximately 0.15 meV 10^{-10} cm^2. This direct pick-up will add a linear term to the chemical potential as we sweep the backgate voltage. The linear contribution from fringing fields to the chemical potential was determined from fitting the chemical potential data at zero magnetic field to the theoretically expected behaviour of the chemical potential with an added linear term. The data in the presence of a magnetic field were then corrected with the linear term stemming from the fringing field.

Received 12 December 2008; accepted 29 June 2009; published online 26 July 2009

References

1. Prange, R. E. & Girvin, S. M. (eds) *The Quantum Hall Effect* (Springer, 1987).
2. Novoselov, K. S. *et al.* Two-dimensional gas of massless Dirac fermions in graphene. *Nature* **438,** 197–200 (2005).

3. Zhang, Y., Tan, Y.-W., Stormer, H. L. & Kim, P. Experimental observation of the quantum Hall effect and Berry's phase in graphene. *Nature* **438,** 201–204 (2005).
4. Ostrovsky, P. M., Gornyi, I. V. & Mirlin, A. D. Theory of anomalous quantum Hall effects in graphene. *Phys. Rev. B* **77,** 195430 (2008).
5. Huckestein, B. Scaling theory of the integer quantum Hall effect. *Rev. Mod. Phys.* **67,** 357–396 (1995).
6. Castro Neto, A. H., Guinea, F., Peres, N. M. R., Novoselov, K. S. & Geim, A. K. The electronic properties of graphene. *Rev. Mod. Phys.* **79,** 109–162 (2009).
7. Ilani, S. *et al.* The macroscopic nature of localization in the quantum Hall effect. *Nature* **427,** 328–332 (2004).
8. Efros, A. L. Non-linear screening and the background density of 2DEG states in magnetic field. *Solid State Commun.* **67,** 1019–1022 (1988).
9. Fogler, M. M., Novikov, D. S. & Shklovskii, B. I. Screening of hypercritical charge in graphene. *Phys. Rev. B* **76,** 233402 (2007).
10. Fogler, M. M. Neutrality point of graphene with coplanar charged impurities. Preprint at <http://arxiv.org/abs/0810.1755> (2008).
11. Struck, A. & Kramer, B. Electron correlations and single particle physics in the integer quantum Hall effect. *Phys. Rev. Lett.* **97,** 106801 (2006).
12. Jain, J. K. *Composite Fermions* (Cambridge Univ. Press, 2007).
13. Nomura, K. & MacDonald, A. H. Quantum Hall ferromagnetism in graphene. *Phys. Rev. Lett.* **96,** 256602 (2006).
14. Alicea, J. & Fisher, M. P. Interplay between lattice-scale physics and the quantum Hall effect in graphene. *Solid State Commun.* **143,** 504–509 (2007).
15. Checkelsky, J. G., Li, L. & Ong, N. P. Divergent resistance at the Dirac point in graphene: Evidence for a transition in high magnetic field. *Phys. Rev. B* **79,** 115434 (2009).
16. Sheng, L., Sheng, D. N., Haldane, F. D. M. & Balents, L. Odd-integer quantum Hall effect in graphene: Interaction and disorder effects. *Phys. Rev. Lett.* **99,** 196802 (2007).
17. Pereira, A. L. C. & Schulz, P. A. Valley polarization effects on localization in graphene Landau levels. *Phys. Rev. B* **77,** 075416 (2008).
18. Geim, A. K. & Novoselov, K. S. The rise of graphene. *Nature Mater.* **6,** 183–191 (2007).
19. Tan, Y.-W. *et al.* Measurement of scattering rate and minimum conductivity in graphene. *Phys. Rev. Lett.* **99,** 246803 (2007).
20. Chen, J.-H. *et al.* Charged impurity scattering in graphene. *Nature Phys.* **4,** 377–381 (2008).
21. Du, X., Skacho, I., Barker, A. & Andrei, E. Y. Approaching ballistic transport in suspended graphene. *Nature Nanotech.* **3,** 491–495 (2008).
22. Bolotin, K. I. *et al.* Ultrahigh mobility in suspended graphene. *Solid State Commun.* **146,** 351–355 (2008).
23. Novoselov, K. S. *et al.* Electric field effect in atomically thin carbon films. *Science* **306,** 666–669 (2004).
24. Novoselov, K. S. *et al.* Two-dimensional atomic crystals. *Proc. Natl Acad. Sci. USA* **102,** 10451–10453 (2005).
25. Schedin, F. *et al.* Detection of individual gas molecules adsorbed on graphene. *Nature Mater.* **6,** 652–655 (2007).
26. Yoo, M. J. *et al.* Scanning single-electron transistor microscopy: Imaging individual charges. *Science* **276,** 579–582 (1997).
27. Yacoby, A., Hess, H. F., Fulton, T. A., Pfeiffer, L. N. & West, K. W. Electrical imaging of the quantum Hall state. *Solid State Commun.* **111,** 1–13 (1999).
28. Zhu, W., Shi, Q. W., Wang, X. R., Chen, J. & Hou, J. G. The shape of disorder broadened Landau subbands in graphene. *Phys. Rev. Lett.* **102,** 056803 (2009).
29. Li, G., Luican, A. & Andrei, E. Y. Scanning tunneling spectroscopy of graphene on graphite. *Phys. Rev. Lett.* **102,** 176804 (2009).
30. Brandt, N. B., Chudinov, S. M. & Ponomarev, Y. G. *Semimetals 1, Graphite and its Compounds* (North-Holland, 1988).
31. Martin, J. *et al.* Observation of electron–hole puddles in graphene using a scanning single electron transistor. *Nature Phys.* **4,** 144–148 (2008).
32. Barlas, Y., Pereg-Barnea, T., Polini, M., Asgari, R. & MacDonald, A. H. Chirality and correlations in graphene. *Phys. Rev. Lett.* **98,** 236601–236604 (2007).
33. Hu, B. Y.-K., Hwang, E. H. & Das Sarma, S. Density of states of disordered graphene. *Phys. Rev. B* **78,** 165411 (2008).
34. Adam, S., Hwang, E. H., Galitski, V. M. & Das Sarma, S. A self-consistent theory for graphene transport. *Proc. Natl Acad. Sci. USA* **104,** 18392–18397 (2007).
35. Zhang, Y., Brar, V. W., Girit, C., Zettl, A. & Crommie, M. F. Origin of spatial charge inhomogeneity in graphene. Preprint at <http://arXiv.org/abs/0902.4793v1> (2009).
36. Deshpande, A., Bao, W., Miao, F., Lau, C. N. & LeRoy, B. J. Spatially resolved spectroscopy of monolayer graphene on SiO_2. *Phys. Rev. B* **79,** 205411 (2009).

Acknowledgements

We would like to acknowledge useful discussions with Y. Meir and A. Auerbach. This work is partly supported by the Harvard NSEC.

Author contributions

J.M.: designing the experiment, sample preparation, measurements, data analysis, preparation of the manuscript. N.A.: measurements, data analysis. G.U.: sample preparation. T.L.: sample preparation. K.v.K.: preparation of the manuscript. J.H.S.: designing the experiment, data analysis, preparation of the manuscript. A.Y.: designing the experiment, data analysis, preparation of the manuscript.

Additional information

Reprints and permissions information is available online at http://npg.nature.com/reprintsandpermissions. Correspondence and requests for materials should be addressed to A.Y.